Supporting Information for:

Unveiling the helicity switching mechanism of a rigid two-tiered stacked architecture

Table S1. Enumeration of 12 possible switching pathways in the helicity inversion of **2T**.

Pathway	Stage I	Stage II	Stage III	Stage IV
No. 1	(*P*)-2T$_{123}$→(*P*)-2T$_{\underline{1}23}$	(*P*)-2T$_{\underline{1}23}$→(*P*)-2T$_{\underline{12}3}$	(*P*)-2T$_{\underline{12}3}$→(*M*)-2T$_{12\underline{3}}$	(*M*)-2T$_{12\underline{3}}$→(*M*)-2T$_{123}$
No. 2	(*P*)-2T$_{123}$→(*P*)-2T$_{1\underline{2}3}$	(*P*)-2T$_{1\underline{2}3}$→(*P*)-2T$_{\underline{12}3}$	(*P*)-2T$_{\underline{12}3}$→(*M*)-2T$_{12\underline{3}}$	(*M*)-2T$_{12\underline{3}}$→(*M*)-2T$_{123}$
No. 3	(*P*)-2T$_{123}$→(*P*)-2T$_{\underline{1}23}$	(*P*)-2T$_{\underline{1}23}$→(*P*)-2T$_{\underline{1}2\underline{3}}$	(*P*)-2T$_{\underline{1}2\underline{3}}$→(*M*)-2T$_{1\underline{2}3}$	(*M*)-2T$_{1\underline{2}3}$→(*M*)-2T$_{123}$
No. 4	(*P*)-2T$_{123}$→(*P*)-2T$_{12\underline{3}}$	(*P*)-2T$_{12\underline{3}}$→(*P*)-2T$_{\underline{1}2\underline{3}}$	(*P*)-2T$_{\underline{1}2\underline{3}}$→(*M*)-2T$_{1\underline{2}3}$	(*M*)-2T$_{1\underline{2}3}$→(*M*)-2T$_{123}$
No. 5	(*P*)-2T$_{123}$→(*P*)-2T$_{1\underline{2}3}$	(*P*)-2T$_{1\underline{2}3}$→(*P*)-2T$_{1\underline{23}}$	(*P*)-2T$_{1\underline{23}}$→(*M*)-2T$_{\underline{1}23}$	(*M*)-2T$_{\underline{1}23}$→(*M*)-2T$_{123}$
No. 6	(*P*)-2T$_{123}$→(*P*)-2T$_{12\underline{3}}$	(*P*)-2T$_{12\underline{3}}$→(*P*)-2T$_{1\underline{23}}$	(*P*)-2T$_{1\underline{23}}$→(*M*)-2T$_{\underline{1}23}$	(*M*)-2T$_{\underline{1}23}$→(*M*)-2T$_{123}$
No. 7	(*P*)-2T$_{123}$→(*P*)-2T$_{\underline{1}23}$	(*P*)-2T$_{\underline{1}23}$→(*M*)-2T$_{1\underline{23}}$	(*M*)-2T$_{1\underline{23}}$→(*M*)-2T$_{1\underline{2}3}$	(*M*)-2T$_{1\underline{2}3}$→(*M*)-2T$_{123}$
No. 8	(*P*)-2T$_{123}$→(*P*)-2T$_{\underline{1}23}$	(*P*)-2T$_{\underline{1}23}$→(*M*)-2T$_{1\underline{23}}$	(*M*)-2T$_{1\underline{23}}$→(*M*)-2T$_{12\underline{3}}$	(*M*)-2T$_{12\underline{3}}$→(*M*)-2T$_{123}$
No. 9	(*P*)-2T$_{123}$→(*P*)-2T$_{1\underline{2}3}$	(*P*)-2T$_{1\underline{2}3}$→(*M*)-2T$_{\underline{1}23}$	(*M*)-2T$_{\underline{1}23}$→(*M*)-2T$_{\underline{1}2\underline{3}}$	(*M*)-2T$_{\underline{1}2\underline{3}}$→(*M*)-2T$_{123}$
No. 10	(*P*)-2T$_{123}$→(*P*)-2T$_{1\underline{2}3}$	(*P*)-2T$_{1\underline{2}3}$→(*M*)-2T$_{\underline{1}23}$	(*M*)-2T$_{\underline{1}23}$→(*M*)-2T$_{12\underline{3}}$	(*M*)-2T$_{12\underline{3}}$→(*M*)-2T$_{123}$
No. 11	(*P*)-2T$_{123}$→(*P*)-2T$_{12\underline{3}}$	(*P*)-2T$_{12\underline{3}}$→(*M*)-2T$_{\underline{1}23}$	(*M*)-2T$_{\underline{1}23}$→(*M*)-2T$_{\underline{1}2\underline{3}}$	(*M*)-2T$_{\underline{1}2\underline{3}}$→(*M*)-2T$_{123}$
No. 12	(*P*)-2T$_{123}$→(*P*)-2T$_{12\underline{3}}$	(*P*)-2T$_{12\underline{3}}$→(*M*)-2T$_{\underline{12}3}$	(*M*)-2T$_{\underline{12}3}$→(*M*)-2T$_{1\underline{2}3}$	(*M*)-2T$_{1\underline{2}3}$→(*M*)-2T$_{123}$

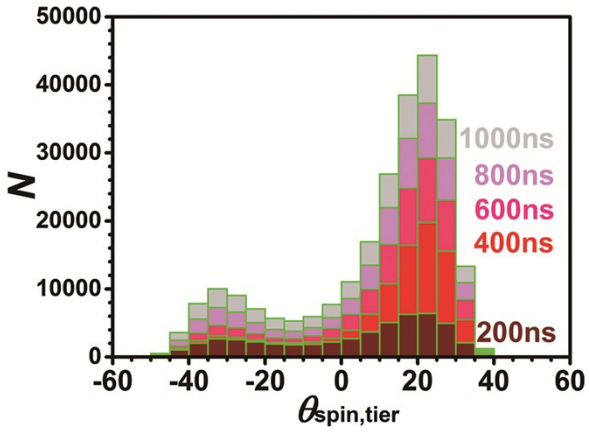

Figure S1. Distributions of the spin angle of the bottom tier relative to the top tier in the 200 ns, 400 ns, 600 ns, 800 ns, and 1.0 μs trajectories of extended adaptive biasing force calculations.

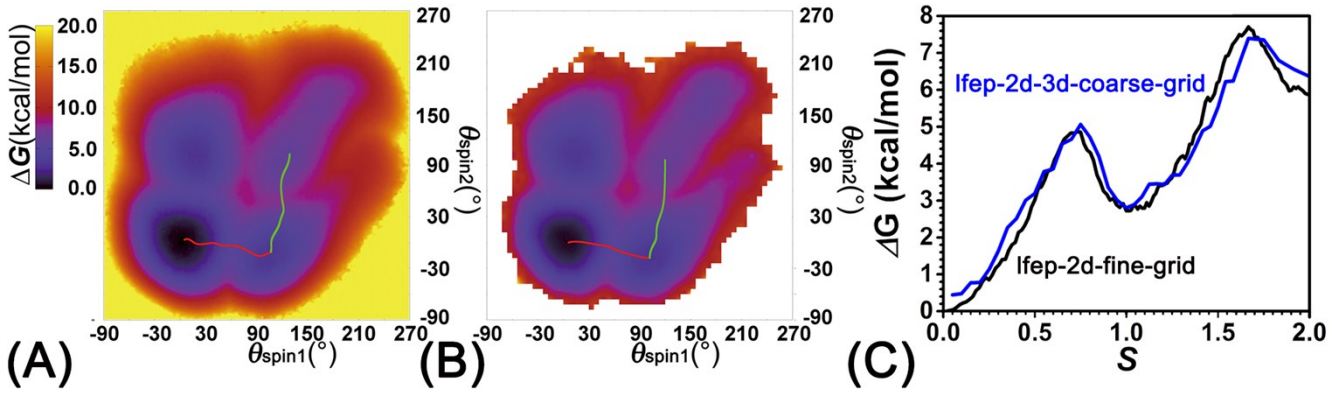

Figure S2. Free-energy landscapes spanned by θ_1 and θ_2 comparing the results of the (A) two- and (B) three-dimensional extended adaptive biasing force calculations. For the three-dimensional case, the landscape is calculated by integration over θ_3 in the range ($-90^o \leq \theta_3 \leq 30^o$). (C) Comparing of least free-energy pathways extracted from results of the two- (black curve) and three-dimensional (blue curve) extended adaptive biasing force calculations.

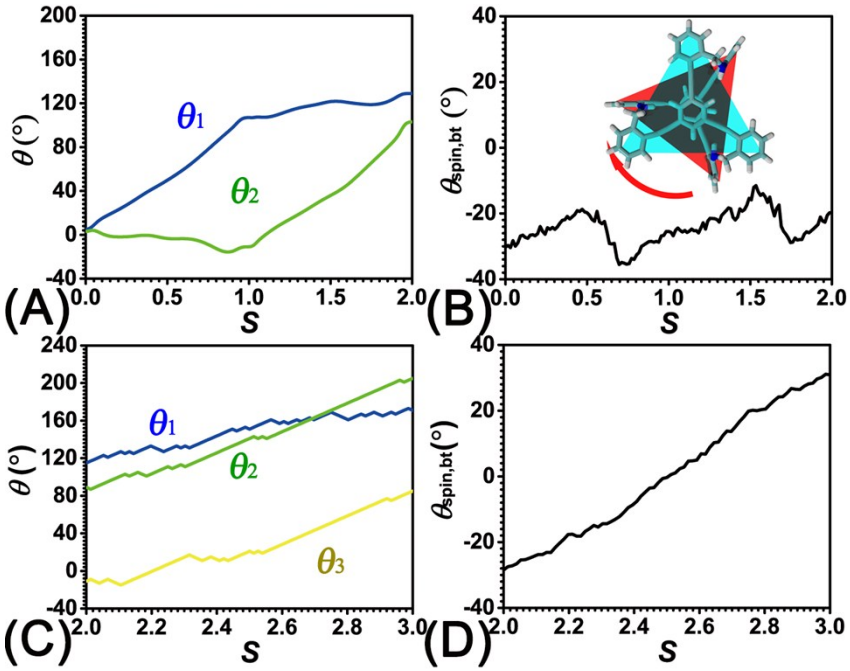

Figure S3. Variation of (A) collective variables (θ_1 and θ_2) and (B) the spin angle of the bottom tier relative to the top tier around *z* axis as a function of position (*s*) along the least free–energy pathway connecting (***P***)-**2T$_{123}$** (*s* = 0.0), (***P***)-**2T$_{\underline{123}}$** (*s* = 1.0), and (***P***)-**2T$_{\underline{123}}$** (*s* = 2.0). Inset of (B): definition of spin angle for the frame of the bottom tier. Variation of (C) collective variables (θ_1, θ_2, and θ_3) and (D) the spin angle of the bottom tier relative to the top tier around *z* axis as a function of position (*s*) along the least free–energy pathway connecting (***P***)-**2T$_{\underline{123}}$** (*s* = 2.0) and (***M***)-**2T$_{\underline{123}}$** (*s* = 3.0).

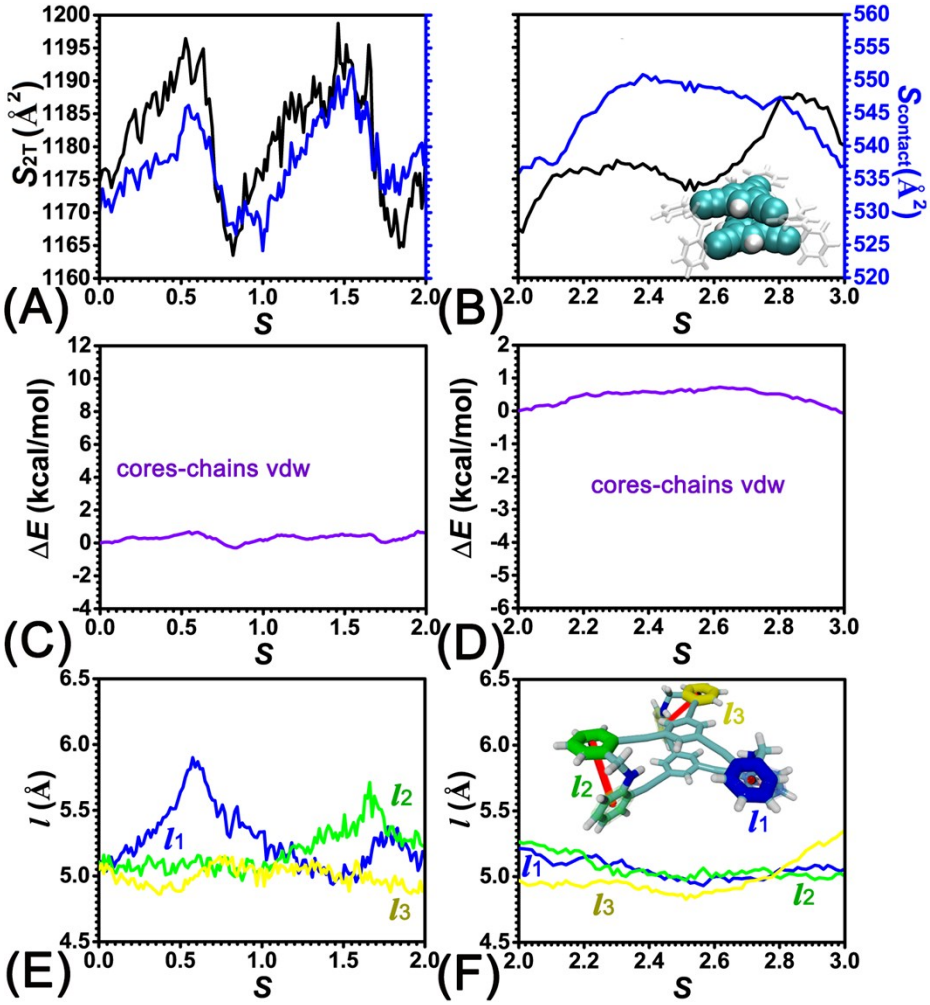

Figure S4. Average solvent accessible surface area of **2T** and its cores in (A) the first, second, and (B) third stages. Inset in (B): definition of the cores (cyan, VDW) and chains (white, Licorice) sections of **2T**. The cores-chains van der Waals term in (E) the first, second, and (F) third stages. Evolution of distances between the center of mass of peripheral rings within the same side chains in (E) the first, second, and (F) third stages.

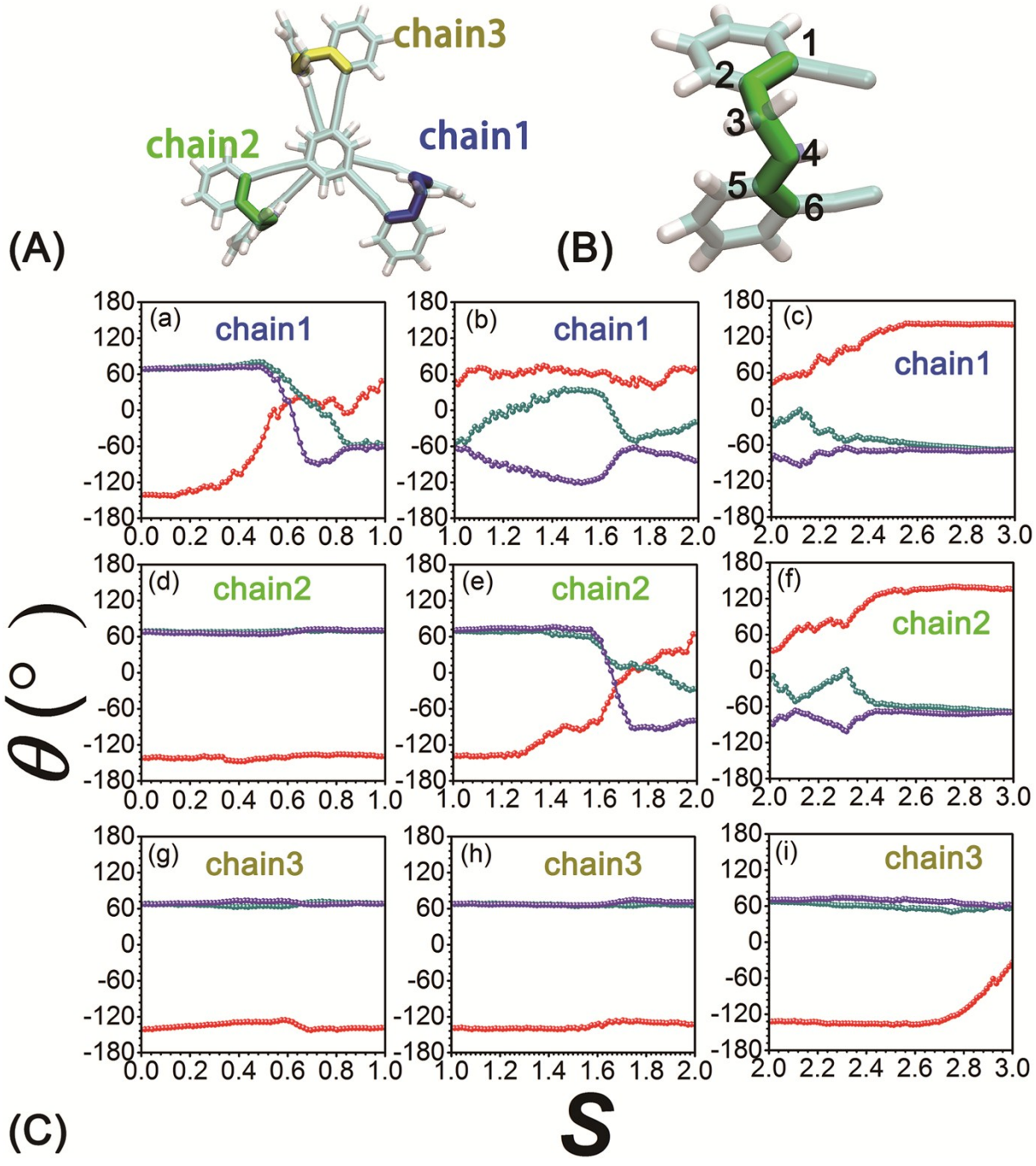

Figure S5. (A) Labels for linkers within **2T**. (B) Labels for atoms involved in one linker. (C) Variation of dihedral angles, (C1-C2-C3-N4) (violet), (C2-C3-N4-C5) (dark cyan), and (C3-N4-C5-C6) (red), within chain1, chain2, and chain3 in the first ($S_{0\rightarrow1}$), second ($S_{1\rightarrow2}$), and third ($S_{2\rightarrow3}$) stages.